

Soft antiphase tilt of oxygen octahedra in the hybrid improper multiferroic $\text{Ca}_3\text{Mn}_{1.9}\text{Ti}_{0.1}\text{O}_7$

Feng Ye,^{1,*} Jinchen Wang,^{2,1} Jieming Sheng,^{2,1} C. Hoffmann,³ T. Gu,^{4,5} H. J. Xiang,^{4,5}
Wei Tian,¹ J. J. Molaison,⁶ A. M. dos Santos,¹ M. Matsuda,¹ B. C. Chakoumakos,¹
J. A. Fernandez-Baca,¹ X. Tong,⁶ Bin Gao,⁷ Jae Wook Kim,⁷ and S.-W. Cheong⁷

¹Quantum Condensed Matter Division, Oak Ridge National Laboratory, Oak Ridge, Tennessee 37831, USA

²Department of Physics, Renmin University of China, Beijing 100872, China

³Chemical and Engineering Materials Division, Oak Ridge National Laboratory, Oak Ridge, Tennessee 37831, USA

⁴Key Laboratory of Computational Physical Sciences, State Key Laboratory of Surface Physics, and Department of Physics, Fudan University, Shanghai 200433, China

⁵Collaborative Innovation Center of Advanced Microstructures, Nanjing 210093, China

⁶Instrument and Source Division, Oak Ridge National Laboratory, Oak Ridge, Tennessee 37831, USA

⁷Rutgers Center for Emergent Materials and Department of Physics and Astronomy, Rutgers University, Piscataway, New Jersey 08854, USA

(Dated: July 23, 2021)

We report a single crystal neutron and x-ray diffraction study of the hybrid improper multiferroic $\text{Ca}_3\text{Mn}_{1.9}\text{Ti}_{0.1}\text{O}_7$ (CMTO), a prototypical system where the electric polarization arises from the condensation of two lattice distortion modes. With increasing temperature (T), the out-of-plane, antiphase tilt of MnO_6 decreases in amplitude while the in-plane, inphase rotation remains robust and experiences abrupt changes across the first-order structural transition. Application of hydrostatic pressure (P) to CMTO at room temperature shows a similar effect. The consistent behavior under both T and P reveals the softness of antiphase tilt and highlights the role of the partially occupied d orbital of the transition metal ions in determining the stability of the octahedral distortion. Polarized neutron analysis indicates the symmetry-allowed canted ferromagnetic moment is less than $0.04 \mu_B/\text{Mn}$ site, despite a substantial out-of-plane tilt of the MnO_6 octahedra.

PACS numbers: 75.58.+t, 81.40.Vw, 75.25.-j, 61.05.F-

Multiferroic compounds with spontaneous elastic, electrical, magnetic orders are considered as the key materials to achieve cross-control between magnetism and electricity in solids with small energy dissipation [1, 2]. The functional properties including colossal magnetoelectric effect could be used in solid-state memories and sensors [3]. The desired multifunctional behavior requires common microscopic origin of the long-range order such that one order parameter is strongly coupled to the conjugate field of the other one. So far, the majority of attention has focused on exploring materials with magnetic origin, where the underlying microscopic mechanisms are primarily classified into three types: symmetric spin exchange interaction $\Sigma_{ij}(\mathbf{S}_i \cdot \mathbf{S}_j)$ [4, 5], antisymmetric spin-exchange interaction $\mathbf{S}_i \times \mathbf{S}_j$ [6, 7], and spin-dependent $p-d$ hybridization due to spin-ligand interaction $(\mathbf{e}_{il} \cdot \mathbf{S}_i)^2 \mathbf{e}_{il}$ [8]. The material-by-design efforts focusing on magnetic oxides has been productive; the ferroelectricity is induced either through epitaxial strain engineering or chemical substitution of stereochemical inactive ions with lone-pair-active cations [9, 10].

However, this approach requires a strong coupling between ferroelectricity and magnetism. The microscopic mechanism with spin origin also implicitly suggests a low operating temperature because of the magnetic frustration. On the other hand, perovskites in the form of ABO_3 and their derivatives are favorably chosen for functional materials due to their high susceptibility toward polar

structural instability and the intimate coupling between the ferroelectric polarization and the magnetic, orbital, and electronic degrees of freedom. Recently, a novel mechanism termed as “hybrid improper ferroelectric” has been proposed to search for materials with spontaneous ferroelectricity. The central idea is that the polar mode is driven by the condensation of two nonpolar lattice modes, which represent oxygen octahedral rotation (X_2^+) and tilt (X_3^-), respectively [11–13]. It is shown that ferroelectricity can be induced experimentally via strain coupling of octahedral rotation between different perovskite heterostructure layers [14] and even realized in bulk materials [11, 15]. Indeed, the higher-order coupling of multidegrees of freedom with the polarization is observed in the Ruddlesden-Popper structures $\text{Ca}_3\text{Ti}_2\text{O}_7$ (CTO) and $\text{Ca}_3\text{Mn}_2\text{O}_7$ (CMO) by neutron powder diffraction [16]. Both compounds exhibit the low-temperature (T) polar $A2_1am$ space group (SG No. 36) that corresponds to symmetry space spanned by two centrosymmetric space groups $Acam$ (No. 64) and $Amam$ (No. 63). In the magnetically ordered CMO, the antiphase octahedral tilt is responsible for the canted moment and suggests a controllable polarization-magnetization coupling via modification of the oxygen octahedral distortion [11, 15]. Thus, instead of searching for materials where the magnetism couples to the electric polarization, the proposal of octahedral-distortion-driven ferroelectricity and magnetoelectricity in this system has shifted the emphasis

to discover room-temperature antiferromagnet $A_3B_2O_7$ compounds [17, 18]. A deeper understanding of the origin for octahedral distortion would provide valuable insight to design materials with optimal performance.

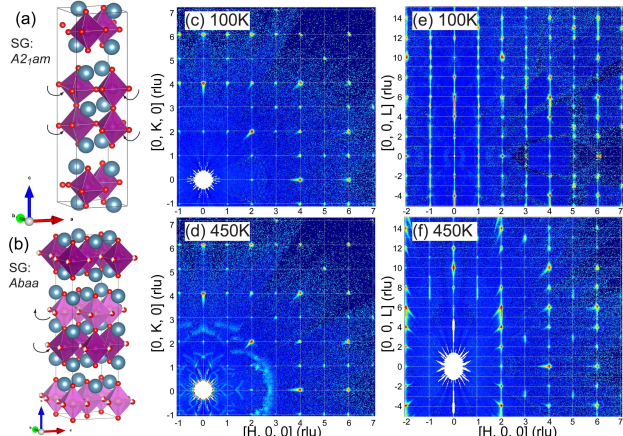


FIG. 1. Crystal structure of $\text{Ca}_3\text{Mn}_{1.9}\text{Ti}_{0.1}\text{O}_7$ in (a) the low- T $A2_1am$ and (b) high- T $Abaa$ phases. The structures are drawn using VESTA software [19]. The diffraction images in the $(h, k, 0)$ scattering plane at (c) 100 K and (d) 450 K. Images in the $(h, 0, l)$ plane at (e) 100 K and (f) 450 K.

In this Rapid Communication, we report an active control of the octahedral distortion of a prototypical hybrid improper multiferroic $\text{Ca}_3\text{Mn}_{1.9}\text{Ti}_{0.1}\text{O}_7$ (CMTO) using temperature (T) and pressure (P). Introducing small amounts of Ti stabilized the crystal growth while keeping the physical properties similar to the pure CMO. We found the antiphase tilt of MnO_6 decreases in amplitude while the inphase rotation remains nearly unchanged with increasing temperature. Hydrostatic pressure has a similar effect; it suppresses the antiphase tilt and has minimal influence on the inphase rotation. The consistent behavior of two distortion modes with respect to both T and P reveals the mechanism contributing to the distortion instability and indicates the ferroelectricity of CMTO can be controlled indirectly by the amplitude of the octahedral distortion.

Single crystals of CMTO were grown using the traveling floating zone method. The chemical compositions were determined by x-ray and neutron diffraction refinements independently and physical properties were characterized by resistivity, and magnetization measurements. Single crystal x-ray diffraction data were collected using a Rigaku XtaLAB PRO diffractometer at the Oak Ridge National Laboratory. Extensive neutron scattering measurements were performed using instruments at the Spallation Neutron Source (SNS) and the High Flux Isotope Reactor (HFIR). Structure analysis was performed using the TOPAZ diffractometer at SNS with crystal size of $2.5 \times 2.5 \times 0.25 \text{ mm}^3$. Large pieces were used to study the thermal evolution of specific reflections using the single crystal diffuse scattering spectrometer CORELLI at

SNS, and the HB1A triple-axis spectrometer at HFIR. Polarized neutron diffraction was performed on a sample with mass $\sim 200 \text{ mg}$ using the HB1 triple axis spectrometer. Heusler crystals were used as the monochromator and analyzer for the polarization setup with flipping ratio of 15 at incident energy $E_i = 13.5 \text{ meV}$. High pressure neutron diffraction was carried out at the SNAP instrument at SNS. An oriented crystal was loaded inside the Paris-Edinburgh pressure cell with lead powder serving as the pressure transmitting medium and gauge.

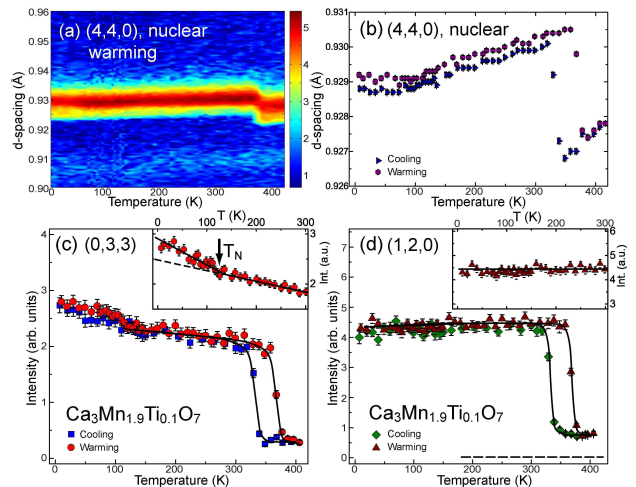


FIG. 2. (a) The T dependence of the nuclear $(4,4,0)$ reflection. (b) Comparison of the d spacing of the same peak on cooling and warming. (c) The T dependence of $(0,3,3)$ reflection associated with the out-of-plane octahedral tilt. (d) The T dependence of the $(1,2,0)$ peak from the in-plane rotation. Insets of panels (c) and (d) show the zoom-in part near the antiferromagnetic transition.

Although the CMO crystal is known to have a non-centrosymmetric $A2_1am$ structure below room temperature [20, 21], the evolution pathway from the high- T tetragonal to the low- T orthorhombic phase remains questionable since a direct continuous transition is not consistent with the Landau theory. It was proposed that a certain intermediate phase might exist over a narrow temperature range. A synchrotron x-ray and neutron diffraction study on the powder sample determined the structure above the transition is nonpolar $Abaa$ (No. 68), where the MnO_6 octahedra of the neighboring perovskite block rotate out of phase by the same angle [16]. The subtle structural transition and lack of sensitivity in powder measurements motivates us to carry out a more thorough examination via single crystal neutron diffraction. Figures 1(c)-1(f) compare the reciprocal space images of the single crystal CMTO at 100 and 450 K in various scattering planes. The low- T patterns agree with the reflection condition for the SG $A2_1am$ with Bragg reflections appearing at $k = 2n$ in the $(h, k, 0)$ plane and $h + l = 2n$ in the $(h, 0, l)$ plane [22]. At 450 K, only reflections with

$h = 2n, l = 2n$ appear in the $(h, 0, l)$ plane, while the pattern of the $(h, k, 0)$ plane remains identical as compared to 100 K. The existence of Bragg peaks with $h + k = \text{odd}$ in the $(h, k, 0)$ plane violates the reflection condition for the nonpolar $Abaa$ phase. CMO has an abnormally large temperature window (~ 70 K) where the low- T polar $A2_1am$ phase coexists with the high- T phase [16]. It is possible that the crystal remains in the mixed-phase state even at 450 K. Alternatively, the observed reflection condition suggests a different crystal structure if single phase is assumed. An exhaustive search leads to a polar $Aba2$ SG (No. 41) which allows the MnO_6 in the bilayer block to rotate out-of-phase with different angles. Refinement using such a structural model improves the agreement between the model and data. Full details are given in the Supplemental Material [23]. Nevertheless, a definitive description of the crystal structure above the transition requires complementary experimental techniques, e.g., bulk polarization and imaging techniques like scanning electron microscopy at high temperatures.

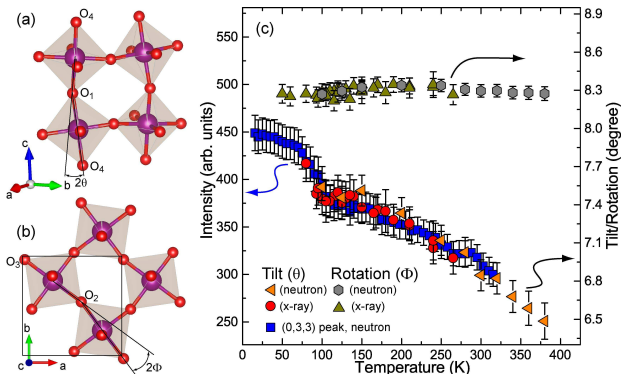


FIG. 3. The schematic diagram of (a) out-of-plane tilt and (b) in-plane rotation of the MnO_6 . (c) The T dependence of refined MnO_6 distortion angles. The T dependence of the $(0,3,3)$ peak intensity from another independent measurement is plotted for comparison.

T dependence of superlattice reflections is used to track the evolution of the structural distortion. As shown in Figs. 2(a) and 2(b), a first-order structural transition is evident near $T_S \sim 370$ K, where the lattice constant experiences an abrupt change with a strong hysteresis. The low- T noncentrosymmetric phase is comprised of an in-plane rotation of MnO_6 octahedra along $[0,0,1]$ (i.e., $a^0a^0c^+$ in Glazer's notation [24]) and a out-of-plane tilt along the $[1,1,0]$ axis in the pseudo-tetragonal setting ($a^-a^-c^0$). We select two characteristic vectors $(1,2,0)$ and $(0,3,3)$ where the scattering structure factors arises from distinct instability modes. Figure 2(c) shows that the peak intensity of the tilt-active $(0,3,3)$ reflection is clearly T -dependent, and decreases steadily with increasing temperature. A change of slope near $T_N \sim 115$ K is discernible [inset of Fig. 2(c)]. In contrast, the intensity of the rotation-active $(1,2,0)$ reflection remains flat be-

low the structural phase transition. The stark difference indicates the rotation of MnO_6 is robust while the tilt is more susceptible to the thermal fluctuation.

The distortions depicted in Figs. 3(a) and 3(b) are quantified by the structural refinement from both x-ray and neutron diffraction [different symbols in Fig. 3(c)]. The inplane rotation and out-of-plane tilt are characterized by the deviation of oxygen sites away from their undistorted positions. The corresponding angles ϕ and θ can be estimated from the refined coordinates, e.g., the rotation angle $\phi = (u_1 - u_2 + v_1 + v_2)$ for the O_2 and O_3 sites located at $(u_1 + 1/2, v_1 + 1/2, w_1)$ and $(u_2, 1 - v_2, w_2)$ [Fig. 3(b)]. The average ϕ is 8.3° in the basal plane, larger than θ which is in the range of 6.5 - 7.7° . Most importantly, the refinement provides compelling evidence that the tilt decreases progressively on warming, while the rotation remains rigid across the whole temperature range. This is in excellent agreement with the diffraction data shown in Figs. 2(c) and 2(d) and the data obtained from another independent sample studied using HB1A.

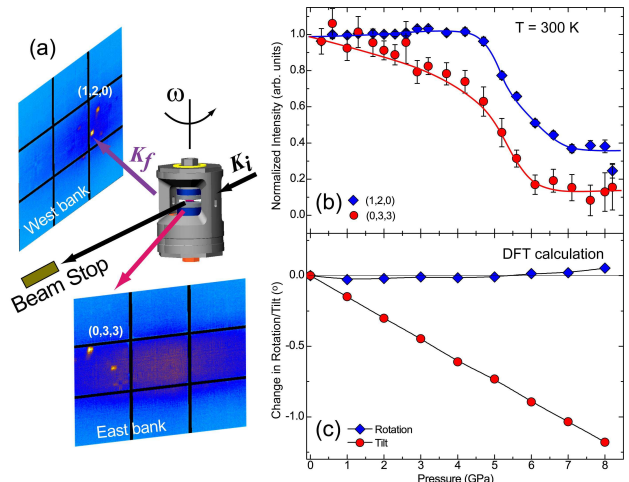


FIG. 4. (a) The pressure experiment setup with the crystal oriented such that the desired reflections can be measured simultaneously using both detector banks. (b) The pressure dependence of $I(P)/I(0)$ of the $(1,2,0)$ and $(0,3,3)$ reflections. Curves are guides to the eye. (c) DFT result of the change of in-phase rotation and antiphase tilt as a function of pressure. The calculation is only performed with structures in the $A2_1am$ phase.

Questions arise as to whether the antiphase tilt is more susceptible to perturbation and whether the observed feature is pertinent only to this particular compound. We thus investigate how the structure responds to the external pressure as it provides an effective tuning parameter to explore the phase diagram. An earlier study of CMO revealed a structural transition from tetragonal to orthorhombic phase near $P \sim 1.3$ GPa [25]. However, the structure in the low- P regime does not agree with the established orthorhombic structure which is likely due to the low sensitivity of x rays to oxygen. To character-

ize the transition, we performed single crystal neutron diffraction under pressure using the SNAP diffractometer. Figure 4(b) plots the intensities of the (1,2,0) and (0,3,3) normalized to the (0,2,2) nuclear Bragg peak that has minimal change across the transition. The (1,2,0) peak intensity associated with octahedral rotation remains nearly unchanged for $P < 4$ GPa while the (0,3,3) intensity is suppressed immediately once the pressure is applied. Both peak intensities decrease at higher pressure and eventually evolve into pressure-independent values for P greater than the critical pressure $P_c \approx 7$ GPa, suggesting the system enters another structure. The P -dependent study further corroborates the softness of the X_3^- tilt mode which responds more dramatically to the stimuli.

The suppression of the antiphase tilt and robustness of the inphase rotation upon increasing T and P in CMTO exhibits distinct differences compared with the isostructural $(\text{Ca}_{1-x}\text{Sr}_x)_3\text{Ti}_2\text{O}_7$, where the antiphase tilt survives against chemical substitution [18]. Previous investigation of the octahedral instability in perovskite oxides has generalized rules to describe the phase transition. (1) The pressure-induced change in octahedral rotation and tilt dR/dP decreases with increasing Goldschmidt tolerance factor (defined as $\tau = (r_A + r_O)/\sqrt{2}(r_B + r_O)$, where r_A , r_B , r_O are radii of the A -, B cations, and O anion) [26, 27]. This has explained the pressure behavior in orthorhombic CaSnO_3 [28], CaTiO_3 [29], and SrTiO_3 [30]. (2) Materials with similar τ show increasing dR/dP as they move from $A^{3+}B^{3+}O_3^{2-}$ to $A^{2+}B^{4+}O_3^{2-}$, and finally to $A^{1+}B^{5+}O_3^{2-}$, which is attributed to the pressure-dependence of the bond-valence parameter. When the A -site cation is at high formal charge, the AO_{12} polyhedron is harder to compress because of its already small A - O distance [31, 32]. Extending to the $A_3B_2O_7$ series, calculation reveals a systematic trend of the distortion amplitudes with respect to τ [33]. The $a^0a^0c^+$ rotation is suppressed, while the $a^-a^-c^0$ tilt remains stable as τ increases. Although CMO and CTO have similar tolerance factors and the same formal charge of the A -site ions, the observation in CMTO does not follow the aforementioned rules and is not consistent with the robustness of the $a^-a^-c^0$ -type tilt mode. Recently, the role of orbital hybridization between the B ions and the oxygen has been suggested to play an important role in determining the octahedral distortion [34]. When pressure is applied on systems containing B ions with empty low-lying d states, the next-nearest neighbor B - O inter-atomic distance is reduced, and the hopping between the O - $2p$ and B - $3d$ orbitals is enhanced significantly, which ultimately leads to the increase of tilt/rotation. In contrast, the partially occupied d orbitals (where there is electron occupation in any of the five d orbitals) will suppress the distortion [34]. This mechanism has successfully explained the contrasting behavior of CaTiO_3 and CaMnO_3 under pressure (see Supplementary Material [23]). We apply similar density

functional theory (DFT) calculation to $\text{Ca}_3\text{Mn}_2\text{O}_7$ and the results are shown in Fig. 4(c). Upon increasing pressure, the antiphase tilt is significantly suppressed and the inphase rotation of MnO_6 shows signs of slightly increasing. The nice agreement between calculation and experimental data reveals the partially occupied d orbitals of the Mn sites are indeed critical for the stability of the MnO_6 distortion. Furthermore, the contradictory pressure behavior between in-phase rotation and antiphase tilt hints at the competition between the two and a presence of trilinear coupling involving both octahedral distortion and the antipolar distortion mode [34].

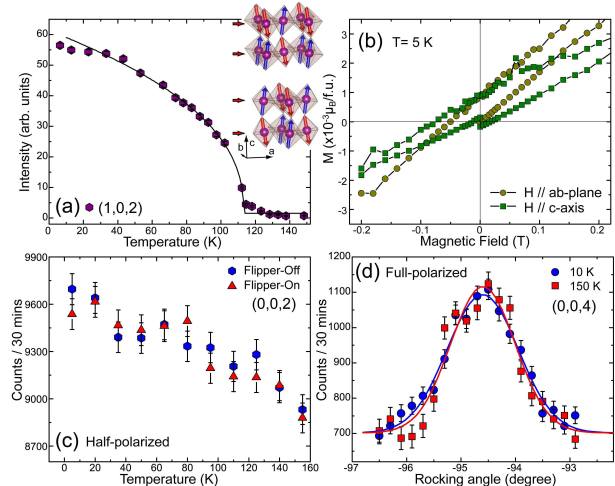


FIG. 5. (a) T dependence of the (1,0,2) magnetic reflection from the G -type AFM order. Inset shows the symmetry-allowed spin configuration. A canted magnetic structure leads to a ferromagnetic component along the a axis. (b) Magnetization measurement with field perpendicular and parallel to the ab plane. (c) T dependence of the (0,0,2) peak with half-polarization setup. (d) Comparison of the scans across the (0,0,4) reflection at 10 and 150 K with full-polarization setup.

CMTO enters antiferromagnetic (AFM) order at $T_N = 115$ K and the moments are dominantly along the c axis [Fig. 5(a)]. The octahedral distortion is directly coupled to the magnetic order and additional spin-orbit interaction (SOI) gives rise to a canted moment of $0.06 \mu_B/\text{site}$ according to the first principles calculation or $0.4 \pm 0.2 \mu_B$ from neutron powder study [21]. The symmetry-allowed weak ferromagnetism (F) results from the trilinear coupling between the G -type AFM, the tilt X_3^- , and F in the lowest-order magnetoelastic coupling approximation. The energy gain is of $V_{MX} \sim -G_c(\mathbf{q}_1)F_bX_3^-(\mathbf{q}_1) + G_c(\mathbf{q}_2)F_aX_3^-(\mathbf{q}_2)$, where a, b, c denote the crystallographic axes, and $\mathbf{q}_1, \mathbf{q}_2$ are the ordering vectors $(1/2, 1/2, 0)$ and $(1/2, -1/2, 0)$ [15]. Since ferromagnetic scattering overlaps with the nuclear scattering, polarized neutron measurement is used to differentiate between the magnetic and nuclear contributions. The (0,0,2)/(0,0,4) peaks are chosen for their large ratio of

the magnetic over nuclear structure factor. In the half-polarization configuration, the intensity is proportional to the summation of nuclear and magnetic scattering in the flipper-off channel, and becomes the difference between the two when the flipper is turned on. The T dependence of the (0,0,2) reflection in both configurations shows no difference within standard error and no anomaly near the AFM transition [Fig. 5(c)]. We also employed full polarization analysis where the scattering intensity is dominantly magnetic in the spin-flip (SF) configuration with polarization parallel to the moment transfer. In Fig. 5(d), the scan profiles in the SF channel at $T = 5$ and 150 K (above T_N) are essentially the same indicating the peak originates mainly from the nuclear scattering leakage in the SF channel. Based on the statistics of the (0,0,4) and other measured nuclear reflections, the upper-bound of the ferromagnetic moment is determined to be $M_s = 0.04 \mu_B/\text{Mn}$. Such a small value is somewhat unexpected when the antisymmetric Dzyaloshinsky-Moriya interaction could lead to a sizable canting moment [35, 36], but consistent with magnetization measurement [Fig. 5(b)], where the obtained moment is in the order of $10^{-3} \mu_B$ per formula unit [37, 38]. A reasonable explanation is the weak SOI associated with the $3d$ Mn ion compared to $5d$ -electron iridates [39]. Although small, the unambiguous existence of the canted moment in conjunction with the soft oxygen octahedral tilt mode offers a feasible strategy to achieve magnetoelectricity control in this layered perovskite, i.e., switching the direction of net moment with electric field [18, 40].

In summary, we performed a systematic neutron and x-ray diffraction study characterizing the structural evolution of the hybrid improper multiferroic CMTO. We identified that the magnitude of the antiphase tilt of the MnO_6 octahedron decreases with increasing temperature and pressure, while the inphase rotation remains stable. We attribute the suppression of antiphase octahedral tilt to the partially occupied d orbitals of the Mn^{4+} ions, in contrast with enhancement of both antiphase and inphase distortion in CTO which only has an empty d orbital at the Ti^{4+} site. The canted ferromagnetic moment has an upper limit of $0.04 \mu_B$ despite substantial MnO_6 tilt. Our study indicates that the active control of the octahedral distortion provides a generic route for designing new ferroelectrics and multifunctional materials.

Research at ORNL was sponsored by the Scientific User Facilities Division, Office of Basic Energy Sciences, U.S. Department of Energy. The work at Rutgers University was supported by the DOE under Grant No. DE-FG02-07ER46382. J.C.W. and J.M.S. acknowledge support from China Scholarship Council. This work has been partially supported by UT-Battelle, LLC under Contract No. DE-AC05-00OR22725 for the U.S. Department of Energy.

-
- * yefl@ornl.gov
- [1] S. W. Cheong and M. Mostovoy, *Nature Materials* **6**, 13 (2007).
 - [2] Y. Tokura, S. Seki, and N. Nagaosa, *Rep. Prog. Phys.* **77**, 076501 (2014).
 - [3] N. Lee *et al.*, *Physical Review Letters* **110**, 137203 (2013).
 - [4] N. Hur *et al.*, *Nature* **429**, 392 (2004).
 - [5] H. J. Xiang, E. J. Kan, Y. Zhang, M. H. Whangbo, and X. G. Gong, *Physical Review Letters* **107**, 157202 (2011).
 - [6] H. Katsura, N. Nagaosa, and A. V. Balatsky, *Physical Review Letters* **95**, 057205 (2005).
 - [7] M. Mostovoy, *Physical Review Letters* **96**, 067601 (2006).
 - [8] T. H. Arima, *Journal of the Physical Society of Japan* **76**, 073702 (2007).
 - [9] J. Wang *et al.*, *Science* **299**, 1719 (2003).
 - [10] G. Catalan and J. F. Scott, *Advanced Materials* **21**, 2463 (2009).
 - [11] N. A. Benedek and C. J. Fennie, *Physical Review Letters* **106**, 107204 (2011).
 - [12] N. A. Benedek, A. T. Mulder, and C. J. Fennie, *J. Solid State Chem.* **195**, 11 (2012).
 - [13] N. A. Benedek, J. M. Rondinelli, H. Djani, P. Ghosez, and P. Lightfoot, *Dalton Transactions* **44**, 10543 (2015).
 - [14] E. Bousquet *et al.*, *Nature* **452**, 732 (2008).
 - [15] A. B. Harris, *Phys Rev B* **84**, 064114 (2011).
 - [16] M. S. Senn *et al.*, *Physical Review Letters* **114**, 035701 (2015).
 - [17] M. J. Pitcher *et al.*, *Science* **347**, 420 (2015).
 - [18] Y. S. Oh, X. Luo, F.-T. Huang, Y. Wang, and S.-W. Cheong, *Nature materials* **14**, 407 (2015).
 - [19] K. Momma and F. Izumi, *Journal of Applied Crystallography* **44**, 1272 (2011).
 - [20] N. Guiblin, D. Grebille, H. Leligny, and C. Martin, *Acta Crystallogr. Sect. C-Cryst. Struct. Commun.* **58**, I3 (2002).
 - [21] M. V. Lobanov *et al.*, *Journal of Physics-Condensed Matter* **16**, 5339 (2004).
 - [22] The structural refinement determines that single crystal used in the measurement has one twinned domains rotating 90 degree along the c -axis, the volume fraction ratio between the primary and twinned domain is 55:45.
 - [23] See Supplemental Material for further details of sample characterization, the temperature evolution of refined parameters below the structural transition, structure at 420 K, and calculation of distortion under pressure for CMTO, which includes Refs.41–52.
 - [24] A. M. Glazer, *Acta Crystallographica Section B-Structural Science* **B 28**, 3384 (1972).
 - [25] J. L. Zhu, R. C. Yu, F. Y. Li, and C. Q. Jin, *Phys. Status Solidi A-Appl. Res.* **194**, 159 (2002).
 - [26] V. M. Goldschmidt, *Naturwissenschaften* **14**, 477 (1926).
 - [27] G. A. Samara, T. Sakudo, and K. Yoshimitsu, *Physical Review Letters* **35**, 1767 (1975).
 - [28] J. Zhao, N. L. Ross, and R. J. Angel, *Phys. Chem. Miner.* **31**, 299 (2004).
 - [29] M. Guennou *et al.*, *Phys Rev B* **82**, 134101 (2010).
 - [30] M. Guennou, P. Bouvier, J. Kreisler, and D. Machon, *Phys Rev B* **81**, 054115 (2010).
 - [31] R. D. Shannon, *Acta Crystallogr. Sect. A* **32**, 751 (1976).
 - [32] R. J. Angel, J. Zhao, and N. L. Ross, *Physical Review*

- Letters **95**, 025503 (2005).
- [33] A. T. Mulder, N. A. Benedek, J. M. Rondinelli, and C. J. Fennie, *Advanced Functional Materials* **23**, 4810 (2013).
- [34] H. J. Xiang, M. Guennou, J. Íñiguez, J. Kreisel, and L. Bellaiche, *Phys Rev B* **96**, 054102 (2017).
- [35] I. Dzyaloshinsky, *Journal of Physics and Chemistry of Solids* **4**, 241 (1958).
- [36] T. Moriya, *Physical Review* **120**, 91 (1960).
- [37] W. H. Jung, *Journal of Materials Science Letters* **19**, 2037 (2000).
- [38] W. K. Zhu, L. Pi, Y. J. Huang, S. Tan, and Y. H. Zhang, *Applied Physics Letters* **101**, 192407 (2012).
- [39] F. Ye *et al.*, *Phys Rev B* **87**, 140406 (2013).
- [40] B. Gao *et al.*, *Applied Physics Letters* **110**, 222906 (2017).
- [41] J. Zikovsky, P. F. Peterson, X. P. P. Wang, M. Frost, and C. Hoffmann, *Journal of Applied Crystallography* **44**, 418 (2011).
- [42] A. J. Schultz *et al.*, *Journal of Applied Crystallography* **47**, 915 (2014).
- [43] A. J. Schultz, K. Srinivasan, R. G. Teller, J. M. Williams, and C. M. Lukehart, *Journal of the American Chemical Society* **106**, 999 (1984).
- [44] A.C. Larson and R.B. Von Dreele, *General Structure Analysis System (GSAS)*, Los Alamos National Laboratory Report LAUR 86-748 (1994).
- [45] G. Sheldrick, *Acta Crystallogr. Sect. A* **64**, 112 (2008).
- [46] P. E. Blöchl, *Phys Rev B* **50**, 17953 (1994).
- [47] G. Kresse and D. Joubert, *Phys Rev B* **59**, 1758 (1999).
- [48] G. Kresse and J. Furthmüller, *Phys Rev B* **54**, 11169 (1996).
- [49] G. Kresse and J. Furthmüller, *Comput. Mater. Sci.* **6**, 15 (1996).
- [50] J. P. Perdew, K. Burke, and M. Ernzerhof, *Physical Review Letters* **77**, 3865 (1996).
- [51] A. I. Liechtenstein, V. I. Anisimov, and J. Zaanen, *Phys Rev B* **52**, R5467 (1995).
- [52] L. Bellaiche and J. Íñiguez, *Phys Rev B* **88**, 014104 (2013).